

Monte Carlo optimization of pair distribution functions: Application to the electronic structure of disordered metals

D. M. Nicholson,* A. Chowdhary, and L. Schwartz†

Department of Physics, Brandeis University, Waltham, Massachusetts 02254

(Received 29 July 1983)

We show that the random-number-based annealing techniques of statistical physics can be used to obtain two site distribution functions that are suitable for use in connection with electronic structure computations based on the muffin-tin model for structurally disordered metals. To illustrate this procedure, we study the temperature dependence of the density of states and electrical resistivity of liquid Cu. Our first-principle calculations predict reasonable values for the negative temperature coefficient of the resistivity (for the appropriate range of Fermi energies) and thus provide support for the Faber-Ziman semiempirical model.

INTRODUCTION

In a series of recent papers we have shown that the effective-medium approximation¹ (EMA) provides a satisfactory description of the electronic properties of structurally disordered metallic systems.²⁻⁵ In particular, we have focused our attention on energy regimes in which the electrons undergo strong scattering that is either *atomic* or *structural* in origin. Examples of the atomic case are *d* states in noble and transition metals,^{2,4} while the structural case is illustrated by electrons whose effective wave vectors, k , are roughly equal to $K_p/2$, where K_p specifies the location of the principal peak in the structure function $s(K)$.³

Within the framework of the muffin-tin model, EMA calculations proceed in terms of three input units: (1) the atomic potentials, (2) the average atomic density n , and (3) the radial distribution function $g(R)$. The first of these ingredients is constructed theoretically by one of a number of different techniques and will not be of direct interest in the present paper. We focus here on the second two units, both of which are, in principle, available from experiment.⁶ In particular, x-ray-diffraction measurements directly yield $s(K)$, and $g(R)$ is then obtained via the Fourier transform

$$g(R) \equiv 1 + h(R) = 1 + \frac{1}{n} \int e^{i\vec{k}\cdot\vec{R}} h(K) \frac{d^3K}{(2\pi)^3} \quad (1a)$$

$$\equiv 1 + \frac{1}{n} \int e^{i\vec{k}\cdot\vec{R}} [s(K) - 1] \frac{d^3K}{(2\pi)^3}. \quad (1b)$$

It should be understood that the functions $h(R)$ and $h(K)$ defined above satisfy certain constraints. Because the atomic spheres surrounding neighboring atoms are non-overlapping, we require

$$h(R) = -1, \quad r < \sigma, \quad (2)$$

where σ is a distance roughly equal to twice the muffin-tin radius. On the other hand, in momentum space, $h(K)$ is subject to the inequality⁶

$$h(K) \geq -1. \quad (3)$$

Unfortunately, it is not a simple matter to obtain pairs $[h(R), h(K)]$ that satisfy the constraints (2) and (3) and are also related by the Fourier transformation (1). The problem is that x-ray-diffraction measurements yield data that are (1) subject to experimental uncertainty, and (2) extend over a limited range of momenta (typically, the data are subject to cutoffs at both large and small K). Even the most reasonable extrapolation procedures (in K space) will generally lead to an $h(R)$ that violates (2). If this $h(R)$ is adjusted "by hand" to satisfy (2), its Fourier transform will almost certainly violate (3).

It is clear that the problem described above severely limits the utility of the muffin-tin EMA method.⁷ We show in the following section that the Monte Carlo techniques introduced by Metropolis *et al.*⁸ can be used to overcome this difficulty. The algorithm described there essentially automates the construction of $[h(R), h(K)]$ pairs that are suitable for realistic electronic structure calculations. In the third section we use this method to study the effects of temperature on the electronic spectrum of a prototype *d*-band system. Beginning with experimental data on molten Cu at 1150 and 1600°C,⁶ we compute electronic densities of states and resistivities. Two features of our results are of particular interest. Firstly, within the *d* bands there is noticeably more structure than was indicated by our previous calculations.² (We argue that this structure was suppressed by spurious features of the pair distribution function employed in Ref. 2.) Secondly, if the Fermi energy E_F is assumed to lie in the vicinity of the structure-induced minimum of the average density of states,³ then the resistivity is found to *decrease* as the temperature is *increased*. This behavior is related to the broadening of the principal peak in $s(K)$ and is consistent with the Faber-Ziman⁹ description of negative temperature coefficients in liquid and amorphous metals.¹⁰ However, in the present case no assumptions regarding the behavior of the effective Fermi wave vector, k_F , are required.

MONTE CARLO OPTIMIZATION

In practice, it is convenient to eliminate $h(R)$ in favor of $H(R) \equiv Rh(R)$. The conditions to be satisfied by the pair $[H(R), h(K)]$ are

$$H(R) \begin{cases} = -R, & R < \sigma \\ \geq -R, & R > \sigma \end{cases} \quad (4)$$

$$\lim_{R \rightarrow \infty} H(R) = 0, \quad (5)$$

$$h(K) \geq -1, \quad (6)$$

$$\lim_{K \rightarrow \infty} h(K) = 0, \quad (7)$$

$$h(K) = \frac{4\pi n}{K} \int H(R) \sin(KR) dR. \quad (8)$$

In Monte Carlo optimization schemes one seeks a vector V (in an abstract space) that minimizes an objective function $E\{V\}$.¹¹ The basic steps of the process are the following. (1) a random change in V is proposed, (2) the change in the objective function $\Delta E\{V\}$ is computed, and (3) the proposed change in V is accepted with a probability

$$p = \begin{cases} 1, & \Delta E < 0 \\ e^{-\Delta E/T}, & \Delta E > 0 \end{cases} \quad (9)$$

where T is an effective temperature. For a given T , these steps are repeated until fluctuations in E are small. The process begins at a temperature T greater than the largest ΔE expected; by slowly reducing T , the system is "annealed" toward the state of minimum E . To apply this technique to the construction of suitable pairs $[H(R), h(K)]$, we begin with an experimental $h_0(K)$ that satisfies (6) and (7) (after careful extrapolation to large and small K). The transform, $H_0(R)$, of $h_0(K)$ will, in general, not satisfy (4), but can usually be adjusted to do so by setting

$$\tilde{H}_0(R) = \begin{cases} -R, & R < \sigma \\ H_0(R), & R > \sigma. \end{cases} \quad (10)$$

The functions $\tilde{H}_0(R)$ and $\tilde{h}_0(K) \equiv h_0(K)$ satisfy (4)–(7) but not (8). Our objective is to find functions $[H'(R), h'(K)]$ that minimize

$$E\{H'(R)\} = \int P_1(R) [H'(R) - \tilde{H}_0(R)]^2 dR + \int P_2(K) [h'(K) - \tilde{h}_0(K)]^2 dK. \quad (11)$$

Here $P_1(R)$ and $P_2(K)$ are weighting functions which can be designed to place more emphasis on particular ranges of R and K , $H'(R)$ is generated by random changes in $\tilde{H}_0(R)$, and $h'(K)$ is calculated from $H'(R)$ via (8). It is hoped that $[H'(R), h'(K)]$ will satisfy (4)–(8) and differ from $[\tilde{H}_0(R), \tilde{h}_0(K)]$ by amounts that are no greater than the experimental uncertainty. Without going into further detail here (see the Appendix), we illustrate this procedure by considering the case of liquid Cu at 1600°C.¹² In Fig. 1(a) we show $\tilde{H}_0(R)$ and $H_0(R)$. In Fig. 1(b), $\tilde{h}_0(K)$ is compared with the transform of the adjusted function $\tilde{H}_0(R)$ shown in Fig. 1(a). (The unphysical features of the dashed curves in Fig. 1 are indicative of the basic problem described above.) In Fig. 2 the final $[H'(R), h'(K)]$ are

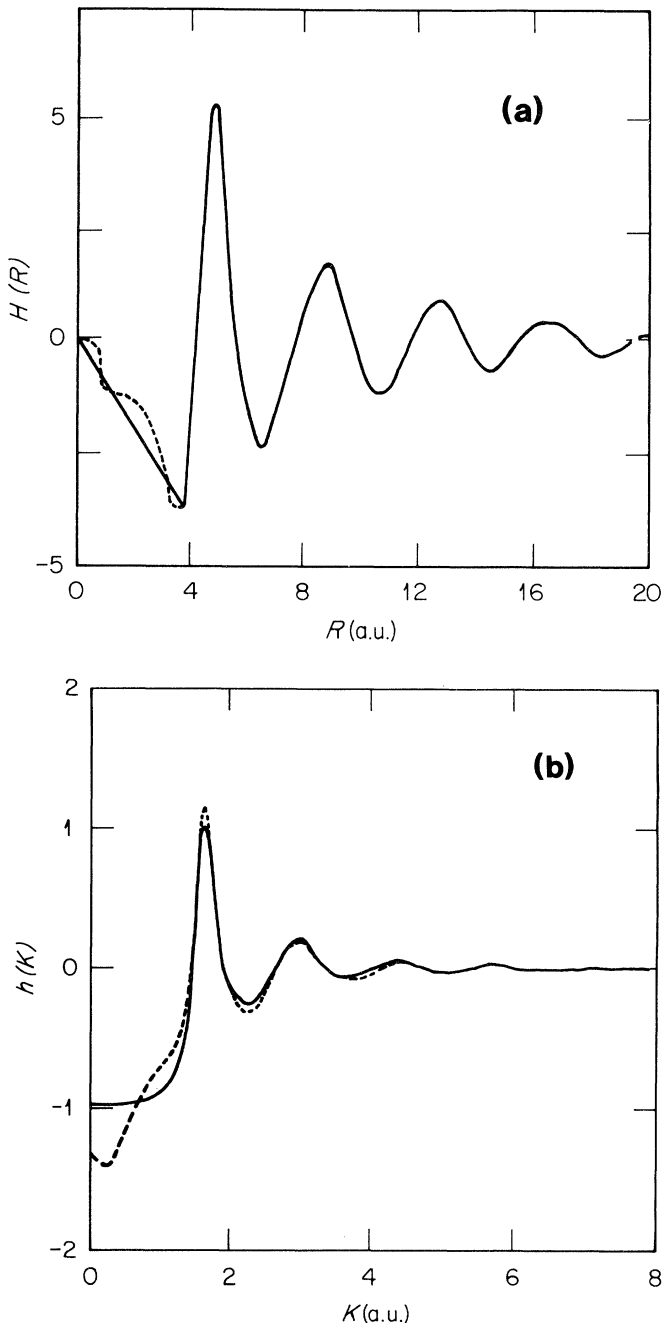


FIG. 1. In (a) are shown $H_0(R)$ (dashed line) [the transform of $\tilde{h}_0(k)$] and $\tilde{H}_0(R)$ (solid line) [defined by (10)]. In (b) we compare $\tilde{h}_0(K)$ (solid line) with the transform of $\tilde{H}_0(R)$ (dashed line).

compared with $[\tilde{H}_0(R), \tilde{h}_0(K)]$. We note that over most of the R and K range the changes introduced by the annealing process are quite small.

TEMPERATURE EFFECTS IN LIQUID Cu

The procedures described above have been used to compute $[H(R), h(K)]$ pairs for liquid Cu at $T=1150$ and

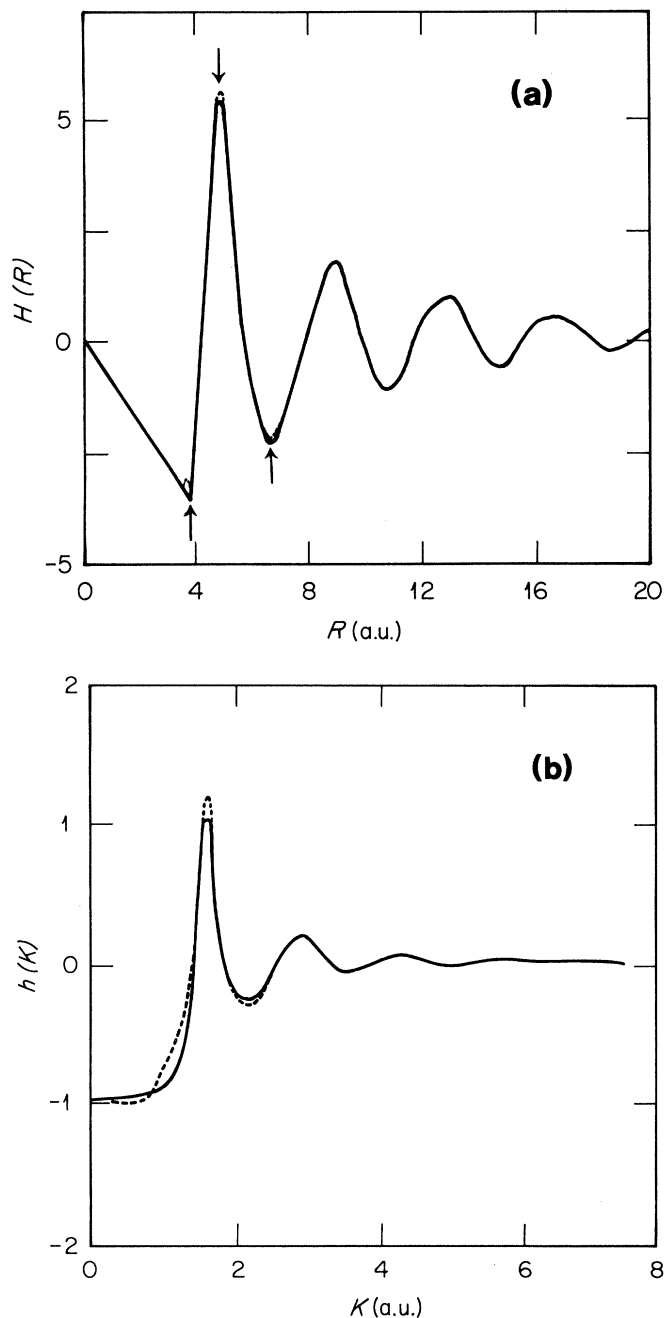


FIG. 2. Converged pair $[H'(R), h'(K)]$ and the objective pair $[\tilde{H}_0(R), \tilde{h}_0(K)]$ are compared. In (a) are shown $\tilde{H}_0(R)$ (solid line) and $H'(R)$ (dash line) [arrows indicate those values of R where $\tilde{H}_0(R)$ and $H'(R)$ differ by more than 1%]; in (b) are shown $\tilde{h}_0(K)$ (solid line) and $h'(K)$ (dashed line).

1600°C.¹² The corresponding EMA densities of states $\rho(E)$ are compared in Figs. 3 and 4 for two energy ranges of interest. In Fig. 3(a) we see that at both temperatures the d bands exhibit a distinct three-peaked structure that can be understood as a smoothed version of the crystalline spectrum. In going from 1150 to 1600°C, the nearest-neighbor peak in $H(R)$ broadens slightly. Since the d states are especially sensitive to local fluctuations, their contribution to the average spectrum is a somewhat

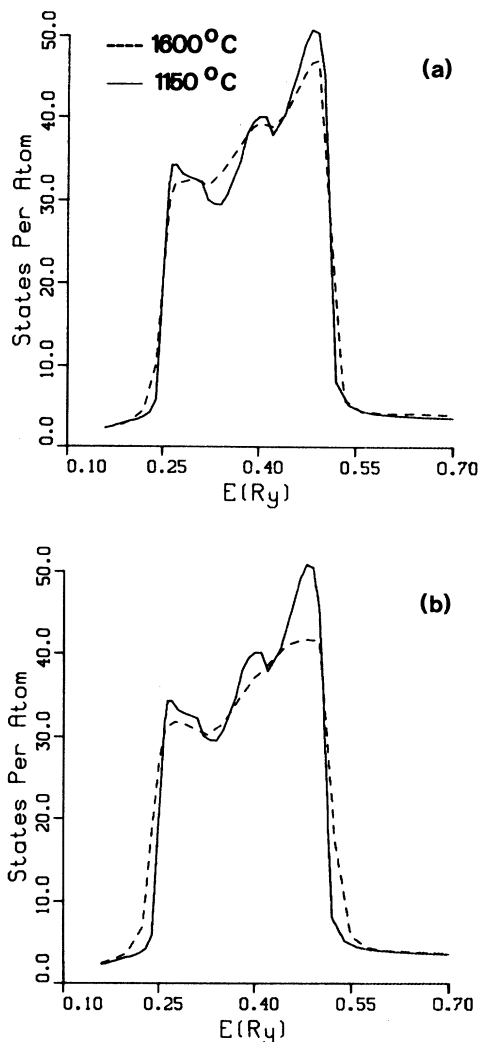


FIG. 3. EMA spectra shown in (a) are based on Monte Carlo-annealed pair distributions for two temperatures. In (b) the present $T = 1150^\circ\text{C}$ spectra (solid line) and the results obtained in Ref. 2 (dashed line) are compared.

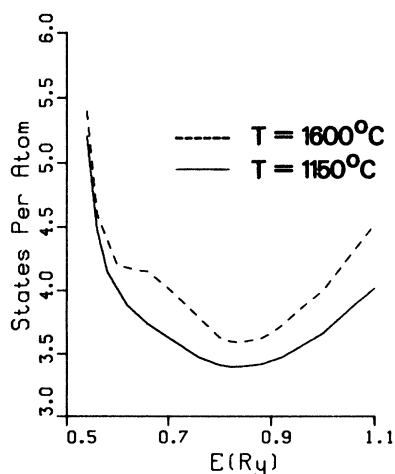


FIG. 4. Structure-induced minima in $\rho(E)$ for $T = 1150$ and 1650°C .

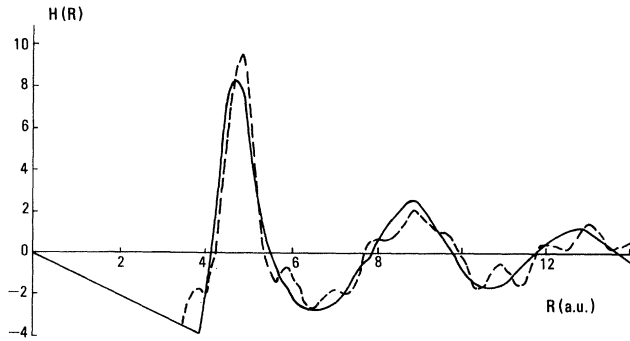


FIG. 5. Monte Carlo-annealed pair distribution for $T = 1150^\circ\text{C}$ (solid line) is compared with the corresponding distribution used in Ref. 2 (dashed line).

smoother function of energy at the higher temperature. In Fig. 3(b) the present results for $T = 1150^\circ\text{C}$ are compared with our previous EMA calculations at that temperature.² Note that the structure within the d band is much less pronounced in our earlier results. The pair distribution function employed in Ref. 2 was based on the same experimental data of Waseda; however, in the earlier calculations, the problems described above were dealt with by a series of modifications introduced "by hand." The $H(R)$ used in Ref. 2 is compared, in Fig. 5, with the one prepared by the techniques developed here. The small oscillations in the dashed curve are spurious consequences of the crude method used to adjust the $[H(R), h(K)]$ pair. One effect of these oscillations is to broaden the distribution of nearest-neighbor distances which would tend to eliminate the structure in the d -band part of $\rho(E)$.

Turning to Fig. 4 we see that increasing the temperature leads to a less well pronounced minimum in the density of states.¹³ Physically, this is expected because, as T increases, the principal peak in $s(K)$ is broadened and the strength of the associated scattering effects is reduced. In Ref. 3 we showed that the EMA spectral density functions

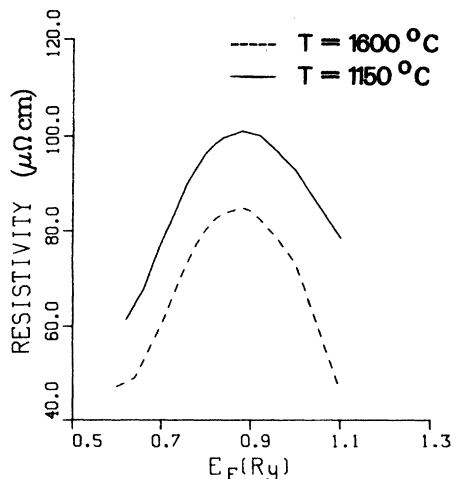


FIG. 6. Electrical resistivities (for E_F within the structure-induced minimum) for $T = 1150$ and 1600°C .

could be used to estimate the dependence of the resistivity on the Fermi energy E_F . In Fig. 6 we show the resistivity maxima calculated for E_F in the vicinity of the structure-induced minimum in $\rho(E)$. Since the scattering is reduced at higher T , it is not surprising that the resistivity is lower at 1600 than at 1150°C . The resulting value for the negative temperature coefficient,

$$\frac{\Delta\rho}{\Delta T} = 0.036$$

measured in $\mu\Omega\text{cm}/^\circ\text{C}$, is quite typical for a range of liquid and amorphous metallic alloys.¹⁰ As we noted in Ref. 3, the effects described in Figs. 4 and 6 are usually interpreted in terms of the empirical Faber-Ziman theory.^{9,14} It is reassuring to see that qualitatively similar results are obtained from the present *ab initio* calculations. Calculations on liquid and amorphous alloys are required before we can claim that a satisfactory description of these effects is in place. Two-component systems require three pair distribution functions, $h_{AA}(R)$, $h_{AB}(R) = h_{BA}(R)$, and $h_{BB}(R)$, but as we have shown in Ref. 4, the methods developed here are readily applicable. Calculations on a prototype transition-metal-metalloid glass are in progress and are planned to be described in a subsequent publication.

ACKNOWLEDGMENTS

This research was supported in part by the National Science Foundation under Grant No. DMR-81-18815.

APPENDIX

The functions $\tilde{H}_0(R)$, $H'(R)$, $\tilde{h}_0(K)$, and $h'(K)$ appearing in Eq. (11) are each stored on uniform N -point grids, where $N = 2^m$, $m < 11$. We denote the spacings on the R and K grids as Δ_R and Δ_K . A typical value for Δ_R is 0.1 a.u. and Δ_K is taken equal to $2\pi/(N\Delta_R)$. The procedure begins with $H'(R) = \tilde{H}_0(R)$; a random point i of the R grid is chosen and the value of $H'(R)$ is changed by an amount ΔH , randomly chosen to be positive or negative,

$$H'(R) = \begin{cases} H'(R), & |R - R_i| > \Delta_R/2 \\ H'(R) \pm \Delta H, & |R - R_i| < \Delta_R/2. \end{cases} \quad (\text{A1})$$

(Here $R_i = i\Delta_R$.) ΔH lies between 0.01 and 0.001 a.u. and its value is fixed throughout the computation. The corresponding change in the objective function is¹⁵

$$\begin{aligned} \Delta E \approx & P_1(R_i) \{ (\Delta H)^2 + 2[H'(R_i) - \tilde{H}_0(R_i)]\Delta H \} \Delta_R \\ & + \sum_j P(K_j) \{ [D(K_j)]^2 \\ & + 2[h'(K_j) - \tilde{h}_0(K_j)]D(K_j) \} \Delta_K, \end{aligned} \quad (\text{A2})$$

where $K_j = j\Delta_K$ and

$$D(K) = 4\pi n \frac{\sin(KR_i)}{K} \Delta H \Delta_R. \quad (\text{A3})$$

The value of $E[\tilde{H}_0(R)]$ is calculated at the outset and at each stage is updated to $E + \Delta E$. This avoids the need to carry out a complete Fourier transform at each stage as might be inferred from Eq. (11). (As a precaution against accumulation of errors, $E[H'(R)]$ is periodically reevaluated from (8) and (11) using a fast Fourier transform.) If we specify $R_i = i\Delta_R$ and $K = j\Delta_K$, where i and j run from 1 to N , Eq. (A3) can be rewritten as

$$D(K) = D(j\Delta_K) = 4\pi n \frac{\Delta_R \Delta H}{K} (-1)^{n_1} \cos \left[n_2 \frac{N}{4} \right], \quad (\text{A4})$$

where n_1 and n_2 ($n_2 < N/2$) are integers defined such that the product $ij = n_1 N/2 + n_2$. Since the cosine function in (A4) needs to be evaluated at only $N/4$ distinct arguments, which can be easily stored, the value of ΔE can be computed quite rapidly and the many iterations required to minimize $E[H'(R)]$ do not require excessive amounts of computer time.

*Present address: Oak Ridge National Laboratory, Oak Ridge, TN 37830.

†Present address: Schlumberger-Doll Research, P.O. Box 307, Ridgefield, CT 06877.

¹L. M. Roth, Phys. Rev. B **9**, 2476 (1974).

²L. Huisman, D. Nicholson, L. Schwartz, and A. Bansil, Phys. Rev. B **24**, 1824 (1981).

³D. Nicholson, and L. Schwartz, Phys. Rev. Lett. **49**, 1050 (1982).

⁴D. Nicholson, L. Huisman, L. Schwartz, A. Bansil, and R. Prasad, Solid State Commun. **46**, 891 (1983).

⁵L. Schwartz, in *Excitations in Disordered Systems*, edited by M. F. Thorpe (Plenum, New York, 1982), p. 177.

⁶Y. Waseda, *The Structure of Non-Crystalline Materials* (McGraw-Hill, New York, 1980). See Chap. 1 for a useful review of the properties of pair distribution functions.

⁷The muffin-tin EMA equations as developed in Ref. 2 [cf. Eqs. (2.3), (2.4), and (2.23) therein] require both $h(R)$ and $h(K)$. These equations are derived by repeated use of the Fourier transform (1).

⁸N. Metropolis, A. W. Rosenbluth, M. N. Rosenbluth, A. H. Teller, and E. Teller, J. Chem. Phys. **21**, 1087 (1953).

⁹T. E. Faber and J. M. Ziman, Philos. Mag. **11**, 153 (1965).

¹⁰Useful reviews of the properties of liquid and amorphous metals are G. Bush and H. -J. Guntherödt, in *Solid State Physics*, edited by H. Ehrenreich, D. Turnbull, and F. Seitz (Academic, New York, 1974), Vol. 29; S. R. Nagel, in *Excitations in*

Disordered Systems, Ref. 5, p. 161.

¹¹Our use of Monte Carlo optimization is perhaps most similar to the work of S. Kirkpatrick, C. D. Gelatt, Jr., and M. P. Vecchi, Science **220**, 671 (1983). A useful review is *Monte Carlo Methods in Statistical Physics*, edited by K. Binder (Springer, Berlin, 1979).

¹²The experimental data employed here was taken from the Appendixes of Ref. 6.

¹³The solid curves in Figs. 4 and 6 differ slightly from the corresponding curves shown in Ref. 3. These differences are again due to changes in the pair distribution function discussed in connection with Fig. 5.

¹⁴Various authors have objected to the Faber-Ziman explanation for the resistivity maximum and the negative resistivity temperature coefficient [M. Jonson and S. M. Girvin, Phys. Rev. Lett. **43** 1447 (1979); Yoseph Imry, *ibid.* **44**, 469 (1979)]. Their objections are based on the fact that the Faber-Ziman equations are (1) based on second-order perturbation theory, and (2) require an *a priori* knowledge of k_F . The results summarized in Figs. 3, 4, and 6 indicate that the present, more complete theory yields results that are in accord with the analysis of Ref. 9.

¹⁵The weighting factors used in our calculations were

$$P_1(R) = \begin{cases} \infty, & R < 0.95\sigma \\ 1, & R > 0.95\sigma \end{cases} \quad P_2(K) = \begin{cases} 100, & K < 0.9 \text{ a.u.} \\ 1, & K > 0.9 \text{ a.u.} \end{cases}$$